PCCP

# Ligated Aluminum Cluster anions, $LAl_n^-$ (n = 1-14, L = $N[Si(Me)_3]_2$)

| | |
|---|---|
| Journal: | *Physical Chemistry Chemical Physics* |
| Manuscript ID | CP-ART-03-2021-001020.R1 |
| Article Type: | Paper |
| Date Submitted by the Author: | 28-Jun-2021 |
| Complete List of Authors: | Liu, Gaoxiang; The Johns Hopkins University, Department of Chemistry<br>Ciborowski, Sandra; The Johns Hopkins University, Department of Chemistry<br>Montone, Georgia ; West Chester University, Department of Physics<br>Sawyer, William; West Chester University, Department of Physics<br>Boggavarapu, Kiran; McNeese State University,<br>Kandalam, Anil; West Chester University, Department of Physics<br>Bowen, Kit; The Johns Hopkins University, Department of Chemistry |
| | |

# Ligated Aluminum Cluster anions, $LAl_n^-$ ($n$ = 1-14, L = $N[Si(Me)_3]_2$)

Gaoxiang Liu,[a#] Sandra M. Ciborowski,[a] Georgia R. Montone,[b] William H. Sawyer,[b]

Boggavarapu Kiran,[c] Anil K. Kandalam,[*b] and Kit H. Bowen[*a]

[a] *Department of Chemistry, Johns Hopkins University, Baltimore, MD 21218, USA*

[b] *Department of Physics & Engineering, West Chester University, West Chester, PA 19383, USA*

[c] *Department of Chemistry and Physics, McNeese State University, Lake Charles, LA 70609, USA*

[#] Present address: *Advanced Bioimaging Center, Department of Molecular and Cell Biology, University of California, Berkeley.*

* Corresponding authors: akandalam@wcupa.edu and kbowen@jhu.edu

## Abstract

A wide range of low oxidation state aluminum-containing cluster anions, $LAl_n^-$ ($n$ = 1–14, L = $N[Si(Me)_3]_2$), were produced via reactions between aluminum cluster anions and hexamethyldisilazane (HMDS). These clusters were identified by mass spectrometry, with a few of them ($n$ = 4, 6, and 7) further characterized by a synergy of anion photoelectron spectroscopy and density functional theory (DFT) based calculations. As compared to a previously reported method which reacts anionic aluminum hydrides with ligands, the direct reactions between aluminum cluster anions and ligands promise a more general synthetic scheme for preparing low oxidation state, ligated aluminum clusters over a large size range. Computations revealed structures in which a methyl-group of the ligand migrated onto the surface of the metal cluster, thereby resulting in "two metal-atom" insertion between Si – $CH_3$ bond.

## Introduction

In recent years, aluminum chemistry has flourished as a result of the major progress in the research on aluminum's low oxidation states (OS).[1-2] These studies started by the advent of low OS aluminum precursors such as Al*X* (*X* = Cl, Br, I, $Cp^*$)[3-8] and largely advanced by utilizing various organic ligands to protect the low OS aluminum compounds.[9-31] Among these ligands, deprotonated pentamethylcyclopentadiene ($Cp^*$) and deprotonated hexamethyldisilazane (HMDS) received special attention.[9-12, 17-31] $Cp^*$ has been reported to protect low OS aluminum compounds of various structures, such as rings and cages,[24-27] and of various stoichiometries, including either aluminum-poor or aluminum-rich clusters.[29-31] The other ligand, deprotonated HMDS, $N[Si(Me)_3]_2$, which is isovalent to $NH_2^-$ and large in size, has also been widely used to protect the central aluminum cluster cores from outer environments. For example, cluster-like $Al_7$, $Al_{12}$, $Al_{69}$, and $Al_{77}$[9-12] with different numbers of $N[Si(Me)_3]_2$ as protective ligands were synthesized using various Al*X* precursors. Studying such clusters can provide insights into the crossover between the molecular species and the bulk metal for main-group elements.[12]

Recently, we extended the study of $Cp^*$- and deprotonated HMDS-ligated aluminum clusters into the gas phase by exploring the reactions between aluminum hydride cluster anions $Al_xH_y^-$ and $Cp^*H$ or HMDS. The formation of and the anion photoelectron spectra of several previously unknown cluster anions, $Cp^*Al_nH^-$ (*n*=1-3)[32] and $LAl_n^-$ (*n* = 2-4, L= $N[Si(Me)_3]_2$)[33], were reported. In these studies, the precursors $Al_xH_y^-$ were generated by a pulsed-arc cluster ion source (PACIS)[34] and then allowed to drift into a beam-gas reaction cell[35] to react with the ligand ($Cp^*H$ or HMDS). The accompanying density functional theory (DFT) based calculations of neutral and anionic LAlH and $LAl_n$ (*n* = 2 – 4) revealed few distinct structural features: (i) the lowest energy isomers were dominated by structures in which the Si-C bond of the ligand molecule was activated by the

$Al_n$ cluster, resulting in at least one aluminum atom being inserted into one of the Si – $CH_3$ bonds of the ligand. ii) As the number of aluminum atoms increased from $n = 2$ to $n = 4$, the additional aluminum atoms preferred to maximize Al – Al interactions by adding peripherally to the existing Al atoms of the smaller systems, i.e., $LAl_{n-1}$. In addition, our measured and calculated vertical detachment energies (VDE) of the ligated-$Al_n^-$ clusters[33] were identical to those of their pure $Al_n^-$ counterparts.[36-38]

In the present work, we adopted a different strategy to generate ligated aluminum clusters in the gas phase: we used a laser vaporization source to make bare aluminum cluster anions $Al_n^-$, and reacted them with HMDS in a reaction cell. Ligated aluminum cluster anions $LAl_n^-$ (L = $N[Si(Me)_3]_2$), where $n$ ranges from 1 to 14, were produced by this approach. Many of these clusters were not observed in our previous work in which we used $Al_xH_y^-$ clusters to react with HMDS.[33] Two new $LAl_n^-$ species, $LAl_6^-$ and $LAl_7^-$, were selected for further analysis by carrying out anion photoelectron spectroscopy and density functional theory (DFT) calculations. Agreement between the experimental and computational vertical detachment energies (VDEs) and adiabatic detachment energies (ADEs) validate the computed structures of these clusters.

## Methods

### Experimental

Anion photoelectron spectroscopy is conducted by crossing a beam of mass-selected negative ions with a fixed-frequency photon beam and energy-analyzing the resultant photo-detached electrons. The photo-detachment process is governed by the energy-conserving relationship: $h\nu$ = EBE + EKE, where $h\nu$ is the photon energy, EBE is the electron binding energy, and EKE is the electron kinetic energy. Our apparatus consists of a laser vaporization cluster anion source with an attached reaction cell, a time-of-flight mass spectrometer, a Nd:YAG photodetachment laser,

and a magnetic bottle electron energy analyzer.[39] The photoelectron spectrometer resolution is ~35 meV at 1 eV EKE. The third (355 nm) harmonic output of a Nd:YAG laser was used to photo-detach electrons from mass-selected $LAl_n^-$ clusters. Photoelectron spectra were calibrated against the atomic transitions of atomic $Cu^-$.[40]

The $LAl_n^-$ clusters were generated using a laser-vaporization/ligation cell source which has been recently applied in our lab for the studies of various molecular reactions.[41] Here, aluminum cluster anions $Al_n^-$ were initially generated by laser vaporization of an aluminum rod. The resultant plasma was cooled with 100 psig of helium gas delivered by a pulsed valve. The resulting aluminum cluster anions then traveled through a reaction cell (4-mm diameter), where they mixed with HMDS vapor. The HMDS vapor was introduced into the reaction cell by a second pulsed valve, which was backed by 15 psig of helium gas. The resulting $LAl_n^-$ anionic clusters were mass-analyzed by the time-of-flight mass spectrometer and their photoelectron spectra were recorded.

**Computational**

The lowest energy isomers of neutral and negatively charged $LAl_n^-$ ($n$ = 5 - 7) clusters were determined by carrying out density functional theory (DFT) based calculations using the Gaussian09 code.[42] The gradient-corrected exchange-correlation functional[43], mPW1PW91 along with 6-311++G(3df,3pd) basis set was used to compute energies of the optimized structures. The accuracy and the reliability of mPW1PW91 functional in predicting the experimental results of $Al_n^-$ clusters have been established in a previously reported theoretical study.[44] In the geometry optimization procedure, the energy convergence criterion was set to $10^{-9}$ Hartree, while the gradient was converged to $10^{-4}$ Hartree/ Å. The vibrational frequencies of all the isomers reported here are positive, thus these isomers correspond to various minima on their corresponding potential energy surfaces.

The vertical detachment energies (VDE) and adiabatic detachment energies (ADE) obtained from the DFT calculations were compared with the corresponding measured values. The VDEs were calculated following the definition VDE = $E_2 - E_1$, where $E_1$ is the total energy of the anion and $E_2$ is the total energy of the neutral, both calculated at the anion's ground state geometry. For the anionic complex with multiplicity $M$, neutral species with multiplicities $M$-1 and $M$+1 were considered in the VDE calculation. The higher transition energies were calculated following the extended Koopmans' theorem[45], in which a correction term $\delta E$, was added to the eigen values of the ground state anion. The correction term $\delta E$ is defined by the equation $\delta E = E_1 - E_2 - \varepsilon_{HOMO}$, where $E_1$ and $E_2$ are the same as discussed above, and $\varepsilon_{HOMO}$ is the eigenvalue of the highest occupied molecular orbital (HOMO) of the anion in its ground state. The adiabatic detachment energy (ADE) is calculated as the energy difference between the lowest energy isomer of the anion and structurally identical isomer (nearest local minimum) of its neutral counterpart. If ground state isomers of the anion and neutral clusters are not significantly different, then the calculated ADE value of the anionic cluster corresponds to the electron affinity (EA) of the corresponding neutral cluster.

## Results and discussion

The mass spectra, with and without HMDS pulsed into the reaction cell, are shown in Figure 1. With no HMDS in the reaction cell, bare aluminum cluster anions, $Al_n^-$, are observed in the mass spectrum; when HMDS is injected into the cell, a new series of ligated aluminum cluster anions $LAl_n^-$ appears, where L is identified as deprotonated HMDS, i.e., $N[Si(Me)_3]_2$. The size of the aluminum core in $LAl_n^-$ ranges from 1 to 14, of which $LAl_5^-$ to $LAl_{14}^-$ have not been observed prior to the current work. This further demonstrates the capability of this laser vaporization–reaction cell setup in preparing various ligated metal cluster anions in the gas phase.[39]

Photoelectron spectra were recorded for three selected $LAl_n^-$ species: $LAl_4^-$, $LAl_6^-$ and $LAl_7^-$systems, and these are displayed in Figure 2. In an anion photoelectron spectrum, the electron binding energy (EBE) value at the peak position in the lowest EBE spectral feature is the vertical detachment energy (VDE), which corresponds to the photo-detachment transition at which the Franck-Condon overlap is maximal between the wave functions of the anion and its neutral counterpart. When there is sufficient Franck-Condon overlap between these two energy states, and when no vibrational hot bands are present, the EA value can be determined as the EBE value at the threshold of the lowest EBE band. Here, the EA values are assigned by extrapolating the low EBE side of the lowest EBE spectral feature to zero intensity.

The $LAl_4^-$ spectrum was taken to compare with the previous $LAl_4^-$ spectrum[33] as a cross-validation, and no significant difference between them can be observed. This demonstrates that the $LAl_n^-$ made in the current work are the same species as those made previously, though they are prepared by reacting HMDS with different low OS aluminum precursors, i.e., bare aluminum cluster anions versus aluminum hydride cluster anions. The photoelectron spectrum of $LAl_6^-$ has a band between 2.2 eV to 3.2 eV, with the first EBE feature starting at about 2.2 eV with several close peaks ranging from 2.6 eV to 3.2 eV. The experimental EA of $LAl_6$ is taken to be 2.2 eV and the experimental VDE of $LAl_6^-$ is 2.62 eV. In the spectrum of $LAl_7^-$, we observe that its lowest EBE band starts at approximately 1.9 eV and reaches maximal intensity at 2.34 eV. Therefore, the EA of neutral $LAl_7$ and the VDE of $LAl_7^-$ are determined as 1.9 and 2.34 eV, respectively. The measured and calculated VDE and ADE values of these systems are given in Table 1.

Even though photoelectron spectrum for $LAl_5^-$ is not reported here, we carried out DFT based calculations and determined the lowest energy isomers of neutral and anionic $LAl_5$ systems (Figure 3). For $LAl_5^-$ cluster, our calculations reveal three nearly energetically-degenerate (within 0.20

eV) structures [Fig. **3a** – **3c**] competing to stabilize the cluster. In the lowest energy structure, isomer **3a**, the $Al_5^-$ moiety forms a distorted triangular bi-pyramid with *one* of its Al atoms inserting between a Si – $CH_3$ bond of the ligand, while another Al atom, bound to the N atom of the ligand, L. This isomer can be considered as an extension of the lowest energy isomer of $LAl_4^-$, reported in our previous study[33]. In isomer **3b**, which is 0.15 eV higher in energy than isomer **3a**, the $Al_5^-$ moiety forms a quasi-planar unit, where in one of the Al atoms is bound to the N atom while another Al atom is inserted into one of the Si – $CH_3$ bonds of the ligand, L. It is noteworthy here that the structure of $Al_5^-$ moiety in **3b** is identical to the previously reported[43] structure of *pure* $Al_5^-$ cluster. The $Al_5^-$ moiety in the third anionic isomer of $LAl_5^-$, **3c** ($\Delta E$ = 0.16 eV), is also structurally similar to the *pure* $Al_5^-$ cluster, albeit with a slight distortion due to its interaction with the ligand. However, unlike in the other isomers of $LAl_5^-$, in isomer **3c**, *two* Al atoms are inserted between the *same* Si – $CH_3$ bond of the ligand. This is the first instance among the $LAl_n^-$ ($n$ = 2 – 5) clusters, where *two* Al atoms are inserted between the same Si – $CH_3$ bond of the ligand. In addition, as we go from $LAl_4^-$ to $LAl_5^-$ cluster, these structures demonstrate a growth pattern where the additional Al atom prefers to bond to other Al atoms, instead of bonding with the ligand directly. All of these anionic isomers prefer a spin multiplicity of doublet (2S+1=2). The calculated VDE values of isomer **3a** are 2.18 eV (corresponding to transition from anionic doublet to neutral singlet) and 2.49 eV (transition from anionic doublet to neutral triplet). For isomer **3b**, wherein the $Al_5^-$ moiety is similar to that of the pure $Al_5^-$ cluster, the calculated VDE values are 2.49 (2 → 1) and 2.51 eV (2 → 3). The calculated VDE values of isomer **3c**, are 2.10 eV (2 →1) and 2.40 eV (2 → 3). It is to be noted here that the measured VDE value of *pure* $Al_5^-$ cluster was reported[45, 46] to be 2.30 eV. Thus, the effect of ligand on the electron binding energy of the $Al_5^-$ seems to be minimal.

The three lowest energy structures of neutral $LAl_5$ are given in Figure 4 [(a) – (c)]. Isomer **4a**, the lowest energy isomer, consists of a quasi-planar $Al_5$ moiety interacting with the ligand, wherein *two* Al atoms are inserted between the Si – $CH_3$ bond, while a third Al atom is bound to the N-atom of the ligand, L. Note that this isomer is similar to isomer **3c**, the higher energy isomer of $LAl_5^-$. Isomer **4b**, which is just 0.12 eV higher in energy than isomer **4a**, consists of $Al_5$ moiety in the shape of distorted triangular bi-pyramid, with its Al atoms inserting between a Si – $CH_3$ bond, while another Al atom, bound to the N atom of the ligand. This isomer is structurally analogous to the lowest energy isomer of $LAl_5^-$ (isomer **3a**). The calculated ADE value of isomer **3a**, calculated as the energy difference between isomer **3a** and its neutral analog, isomer **4b** is 2.00 eV; while the ADE value of isomer **3c**, calculated as the energy difference between isomer **3c** and isomer **4a** is 1.71 eV. Note that our calculations did not reveal a neutral analog of isomer **3b** as it was not a minimum on the potential energy surface of the neutral cluster.

The lowest energy isomers of anionic and neutral $LAl_6$ systems are given in Figure **5**. In the lowest energy isomer of anionic $LAl_6^-$, (isomer **5a**) *two* Al atoms of an $Al_6^-$ octahedral moiety are inserted between a Si – $CH_3$ bond of the ligand, while another Al atom is bound to the N-atom of the ligand, L. The next higher energy isomer ($\Delta E$ = 0.63 eV), isomer **5b**, has only *one* Al atom of a slightly distorted $Al_6^-$ octahedron inserted between a Si – $CH_3$ bond of the ligand. Note that the *pure* $Al_6^-$ cluster also forms an octahedron structure.[43] Interestingly, a structure where *two* Al atoms of the $Al_6^-$ moiety are inserted between two *different* Si – $CH_3$ bonds of the ligand is 0.88 eV higher in energy than isomer **5a**. In this higher energy isomer, the $Al_6^-$ moiety adopted a planar geometry. In addition, the structure in which an $Al_6^-$ octahedron is bound to just the N-atom of the ligand, *without* any Al insertions is 0.82 eV higher in energy than isomer **5a**. Our calculated VDE value of the lowest energy isomer (isomer **5a**) 2.52 eV, while the VDE of next higher energy

isomer (isomer **5b)** is calculated to be 2.40 eV. Both these VDE values are in good agreement with the measured value of 2.6 eV. Note that the measured VDE value of *pure* $Al_6^-$ was reported[45,46] as 2.63 ± 0.06 eV, again indicating that our ligand, L has a minimal effect on the electron binding energy of $Al_6^-$. This is consistent with the observation in our previous study[33] on $LAl_n^-$ ($n$ = 2 – 4) and in $LAl_5^-$. Since the photoelectron spectrum of $LAl_6^-$ consists of a band made up of several peaks ranging from 2.6 to 3.1 eV and to understand how many isomers are contributing towards the first broad peak of the photoelectron spectrum, we calculated the higher transition energies of both the isomers (isomers **5a** and **5b**) by employing extended Koopman's theorem. The next two higher energy transitions are due to the electron detachments from HOMO−1 and HOMO – 2, respectively. In the case of isomer **5a**, these higher transition energies are calculated to be 2.8 eV and 3.10 eV, while in the isomer **5b**, they are 2.70 eV and 3.31 eV. The calculated VDE values and the higher energy transitions of both isomers, **5a** and **5b**. are in good agreement with the observed photoelectron spectra of $LAl_6^-$. Hence, we can report that both these isomers are present in the cluster beam of $LAl_6^-$ and have contributed towards the photoelectron spectrum of $LAl_6^-$ given in Figure 2. However, since the energy of the isomer **5b** is 0.63 eV higher in energy than isomer **5a**, the concentration of isomer **5b** is expected to be significantly lower than that of isomer **5a**.

The lowest energy isomer of neutral $LAl_6$, isomer **5c**, is similar to that of its anionic counterpart, wherein two Al atoms of $Al_6$ octahedron are inserted between a Si-$CH_3$ bond of the ligand, L. The next higher energy isomer ($\Delta E$ = 0.60 eV), isomer **5d**, is similar to isomer **5b**, the higher energy isomer of $LAl_6^-$. The calculated ADE value of isomer **5a** is 2.23 eV, while the ADE of isomer **5b** is 2.20 eV. Since the lowest energy isomers of anionic and neutral $LAl_6$ are identical, we can designate the ADE values of $LAl_6^-$ as the EA of the neutral $LAl_6$. These two values are in

excellent agreement with the measured value of 2.2 eV, thus reinforcing the contribution of both isomers in the photoelectron spectrum of $L\text{Al}_6^-$.

Figure 6 shows the lowest energy isomers of negatively charged and neutral $\text{LAl}_7$ systems. Our calculations reveal two energetically nearly-degenerate ($\Delta E$ = 0.12 eV) structures for $\text{LAl}_7^-$, isomer **6a** and isomer **6b**. The lowest energy isomer of $\text{LAl}_7^-$ (isomer **6a)**, consists of a face-capped octahedral $\text{Al}_7^-$ moiety, with *two* Al atoms inserted between the Si – $\text{CH}_3$ bond of the ligand and the face-capping Al atom bound to the N atom of the ligand, L. In the next higher energy isomer (isomer **6b**), the $\text{Al}_7^-$ moiety forms a face-capped prism structure, with the Al atom capping the square face of the $\text{Al}_6$ prism bound to the N atom of the ligand. In addition, *two* Al atoms are inserted between the Si – $\text{CH}_3$ bond of the ligand. Both these anionic isomers prefer to form a doublet (2S+1 = 2) spin state. The calculated VDE values of isomer **6a** are 2.64 eV (transition from anionic doublet to neutral singlet) and 2.91 eV (transition from anionic doublet to neutral singlet), while the VDE values of isomer **6b** are calculated to be 2.22 eV (2 → 1) and 2.87 eV (2 → 3). Comparing our calculated lowest energy electron detachment values (for transition from anionic doublet to neutral singlet states) of both these isomers with the photoelectron spectrum of $\text{LAl}_7^-$ given in Figure 2, we can say that both isomers are contributing towards the lowest EBE band, which is a result of an overlap of two peaks, one centered around 2.20 eV and the other centered around 2.40 eV. The next higher energy EBE band of the spectrum (see Fig. 2) starts around 2.7 eV and extends to 3.4 eV. Our calculated electron detachment energy values, corresponding to transitions from anionic *doublet* to neutral *triplet* states in both isomers (2.91 and 2.87 eV) are contributing towards this higher energy band. In addition, we have also calculated other higher transition energies using the extended Koopman's theorem. For isomer **6a**, the next three transition energies are 3.00, 3.12, and 3.27 eV; for isomer **6b**, they are 3.00, 3.18, and 3.26

eV. These transitions are all in good agreement with the higher energy EBE band of the $LAl_7^-$ spectrum given in Figure 2. Thus, one can conclude that both isomers **6a** and **6b** are present in the cluster beam and are contributing towards the photoelectron spectrum of $LAl_7^-$. It is to be noted here that the measured VDE value of pure $Al_7^-$ cluster was reported[46, 47] to be 2.30 eV. Thus, the effect of ligand on the electron binding energy of the $Al_7^-$ seems to be minimal.

The lowest energy isomer of neutral $LAl_7$ (isomer **6c**) also consists of a face-capped $Al_7$ octahedron, with *two* of its Al atoms inserted between the Si – $CH_3$ bond. Unlike in the case of the anionic lowest energy isomer (isomer **6a**), in this isomer the face-capping Al atom is bound to the methyl group of the ligand. The next higher energy isomer (isomer **6d**) corresponds to a face-capped $Al_7$ octahedron, but with only *one* Al atom inserted between the Si – $CH_3$ bond. This single-atom inserted isomer (isomer **6d**) is 0.80 eV higher in energy than "two-atom" inserted isomer (isomer **6c**). The calculated ADE value of isomer **6a** is 1.96 eV, which is in good agreement with the experimental ADE value of 1.90 eV.

Having established the ground state isomers of neutral and anionic $LAl_n$ systems, we now turn to understand the interesting structural features of these systems. The ground state structures of neutral and anionic $LAl_n$ ($n$ = 2 – 7) systems can be viewed as a result of the activation of Si-$CH_3$ bond and subsequent *migration* of the methyl group to the rest of the metal cluster. In our earlier reported study[33], it was observed that as we move from $LAl_2^-$ to $LAl_4^-$, the energy difference between the isomer with an Al-atom inserted into the Si-$CH_3$ bond and the isomer without any breaking of Si-$CH_3$ bond, increased from 0.50 eV to 0.68 eV. This clearly indicates an increased preference for structures in which the methyl group of the ligand has migrated to one of the Al atoms of the metal cluster thereby resulting in an Al-atom insertion between Si – $CH_3$. In the current study, as we move from $LAl_5^-$ to $LAl_7^-$, a clear preference for structures with *two* Al atoms

inserted between the Si-$CH_3$ bond (see Figures 3, 5, and 6) emerges. As the aluminum cluster size increased from $Al_5$ to $Al_7$, a single-aluminum atom insertion into Si-$CH_3$ bond has resulted in destabilizing the structural integrity and electron delocalization in the metal cluster (see Fig. **5b** and **5d**). Thus, to maintain the structural integrity and delocalization, the methyl group further migrated to another Al atom of the $Al_n$ cluster, thereby resulting in a more symmetric $Al_n^-$ moiety (see Fig. **5a** and **5c**). This migration has resulted in a more stable structure, which was labeled as "two-atom" inserted isomers.

The four frontier molecular orbitals (MOs) of $LAl_n^-$ ($n$ = 5 - 7) are given in Figure 7. If one considers the $LAl_n^-$ complex as a ligand, L interacting with an aluminum cluster, then the bonding and the molecular orbital composition becomes clear. The frontier bonding orbitals for all the complexes considered here show bonding interactions between the Al atoms in the metal cluster with negligible contributions from the ligand. This is fairly obvious due to the weak bonding between Al-Al atoms in these small cluster range. Since the MO picture show a delocalized bonding pattern within the aluminum cluster, one would anticipate minimal disturbance to bonds as an electron is removed from these MOs with each transition in the photoelectron spectroscopy. NPA charge analysis provides further insight into the nature of these complexes. The charge on the $Al_n$ cluster in the anionic complexes is very small, indicating that the negative charge is mostly located on the ligand. A comparison of the NPA charges on the anionic and neutral $LAl_n$ complexes revealed that during the photo-detachment of the extra electron from the anionic $LAl_n^-$, it is the $Al_n$ moiety that lost majority (>80%) of the charge. Note that a similar pattern was reported in our previous study[33] on $LAl_n$ ($n$ = 2 – 4) complexes.

## Concluding Remarks

A wide range of low-oxidation state aluminum-containing clusters, $LAl_n^-$ ($n$ = 1-14), were generated via the direct reaction between bare aluminum cluster anions and the hexamethyldisilazane molecules. Among them, the geometrical and electronic structure of $LAl_6^-$ and $LAl_7^-$ systems were characterized by using negative ion photoelectron spectroscopy and density functional theory-based calculations. Our computational results show that as the size of the aluminum cluster increased from $n$ = 5 to 7, a $CH_3$-group from the ligand migrated onto the aluminum metal cluster, thus forming structures in which two Al atoms are inserted between Si-$CH_3$ bond. The effect of the ligand on the geometrical and electronic structure of $Al_n$ moiety seems to be minimal, with the $Al_n$ retaining its structural integrity during the interaction with the ligand and the calculated (and measured) electron detachment energies similar to that of the pure $Al_n^-$ clusters.

**Acknowledgements**

This material is based on work supported by the Office of Naval Research (ONR), Multidisciplinary University Research Initiative (MURI) under Grant No. N00014-15-1-2681 and the Air Force Office of Scientific Research (AFOSR) under Grant No. FA9550-19-1-0077 (K. H. B.).

## References


1. W. Roesky and S. S. Kumar, *Chem. Commun.*, 2005, 4027-4038.
2. H. W. Roesky, *Inorg. Chem.*, 2004, **43**, 7284-7293.
3. M. Tacke and H. Schnöckel, *Inorg. Chem.*, 1989, **28**, 2895-2896.
4. M. Mocker, C. Rob and H. Schnöckel, *Angew. Chem.*, 1994, **106**, 1860-1861.
5. A. Ecker and H. Schnöckel, *Z. Anorg. Allg. Chem.*, 1996, **622**, 149-152.
6. C. Dohmeier, C. Roble, M. Tacke and H. Schnöckel, *Angew. Chem.*, 1991, **103**, 594-595.
7. C. Dohmeier, D. Loos and H. Schnöckel, *Angew. Chem.*, 1996, **108**, 141-161.
8. J. Gauss, U. Schneider, R. Ahlrichs, C. Dohmeier and H. Schnöckel, *J. Am. Chem. Soc.*, 1993, **115**, 2402-2408.
9. A. Purath, R. Köppe and H. Schnöckel, *Angew. Chem.*, 1999, **111**, 3114-3116 (*Angew. Chem. Int. Ed.*, 1999, **38**, 2926).
10. A. Purath, R. Köppe and H. Schnöckel, *Chem. Commun.*, 1999, 1933-1934.
11. H. Köhnlein, A. Purath, C. Klemp, E. Baum, I. Krossing, G. Stösser and H. Schnöckel, *Inorg. Chem.*, 2001, **40**, 4830-4838.
12. E. Ecker, E. Weckert and H. Schnöckel, *Nature*, 1997, **387**, 379-381.
13. C. Dohmeier, M. Mocker, H. Schnöckel, A. Lötz, U. Schneider and R. Ahlrichs, *Angew. Chem.*, 1993, **105**, 1491-1493. (*Angew. Chem. Int. Ed.*, 1993, **32**, 1428).
14. A. Schnepf and H. Schnöckel, *Adv. Organomet. Chem.*, 2001, **47**, 235-281.
15. C. Üffing, A. Ecker, R. Köppe, K. Merzweiler and H. Schnöckel, *Chem. Eur. J.*, 1998, **4**, 2142-2147.
16. N. Etkin and D. W. Stephan, *Organometallics*, 1998, **17**, 763-765.

17. S. J. Urwin, D. M. Rogers, G. S. Nichol and M. J. Cowley, *Dalton Trans.*, 2016, **45**, 13695-13699.

18. A. Haaland, K.-G. Martinsen, S. A. Shlykov, H. V. Volden, C. Dohmeier and H. Schnöckel, *Organometallics*, 1995, **14**, 3116-3119.

19. J. D. Gorden, A. Voigt, C. L. B. Macdonald, J. S. Silverman and A. H. Cowley, *J. Am. Chem. Soc.*, 2000, **122**, 950-951.

20. C. Dohmeier, H. Krautscheid and H. Schnöckel, *Angew. Chem.*, 1994, **106**, 2570-2572.

21. C. Üffing, A. Ecker, R. Köppe and H. Schnöckel, *Organometallics*, 1998, **35**, 2373-2375.

22. Q. Yu, A. Purat, A. Douchev and H. Schnöckel, *J. Organomet. Chem.*, 1999, **584**, 94.

23. J. Weiß, D. Stetzkamp, B. Nuber, R. A. Fischer, C. Boehme and G. Frenking, *Angew. Chem. Int. Ed.*, 1997, **36**, 70-72.

24. D. Weiß, T. Steinke, M. Winter, R. A. Fischer, N. Fröhlich, J. Uddin and G. Frenking, *Organometallics*, 2000, **19**, 4583-4588.

25. S. Schulz, T. Schoop, H. W. Roesky, L. Häming, A. Steiner and R. Herbst-Irmer, *Angew. Chem. Int. Ed.*, 1995, **34**, 919-920.

26. C. K. F. von Haenish, C. Üffing, M. A. Junker, A. Ecker, B. O. Kneisel and H. Schnöckel, *Angew. Chem. Int. Ed.*, 1996, **35**, 2875-2877.

27. C. Dohmeier, H. Schnöckel, C. Robl, U. Schneider and R. Ahlrichs, *Angew. Chem. Int. Ed.*, 1994, **33**, 199-200.

28. C. Ganesamoorthy, S. Loerke, C. Gemel, P. Jerabek, M. Winter, G. Frenking and R. A. Fischer, *Chem. Commun.*, 2013, **49**, 2858-2860.

29. J. Vollet, J. R. Hartig and H. Schnöckel, *Angew. Chem. Int. Ed.*, 2004, **43**, 3186-3189.

30. K. Weiß and H. Schnöckel, *Anal. Bioanal. Chem.*, 2003, **377**, 1098.

31. K. S. Williams and J. P. Hooper, *J. Phys. Chem. A*, 2011, **115**, 14100-14109.

32. X. Zhang, G. Gantefoer, B. Eichhorn, D. Mayo, W. H. Sawyer, A. F. Gill, A. K. Kandalam, H. Schnöckel and K. Bowen, *J. Chem. Phys.*, 2016, **145**, 074305 (1 – 6).

33. X. Zhang, L. Wang, G. Montone, A. Gill, G. Gantefoer, B. Eichhorn, A. K. Kandalam and K. H. Bowen, *Phys. Chem. Chem. Phys.*, 2017, **19**, 15541-15548.

34. X. Zhang, G. Liu, G. Gantefoer, K. H. Bowen and A. N. Alexandrova, *J. Phys. Chem. Lett.*, 2014, **5**, 1596-1601.

35. **(a)** X. Zhang, G. Liu, K.-H. Meiwes-Broer, G. Ganteför and K. H. Bowen, *Angew. Chem. Int. Ed.*, 2016, **55**, 9644-9647. **(b)** G. Liu, P. Poths, X. Zhang, Z. Zhu, M. Marshall, M. Blankenhorn, A. N. Alexandrova and K. H. Bowen, *J. Am. Chem. Soc.*, 2020, **142**, 7930-7936.

36. X. Li, H. Wu, X. – B. Wang, and L. – S. Wang, *Phys. Rev. Lett.* 1998, **81**, 1909 – 1912

37. C. Y. Cha, G. Gantefor, and W. Eberhardt, *J. Chem. Phys.* 1994, **100**, 995 – 1010

38. S. R. Miller, N. E. Schultz, D. G. Truhlar, D. G. Leopold, *J. Chem. Phys.* 2009, **130**, 024304

39. G. Liu, S. Ciborowski and K. H. Bowen, *J. Phys. Chem. A*, 2017, **121**, 5817-5822.

40. J. Ho, K. M. Ervin and W. C. Lineberger, *J. Chem. Phys.*, 1990, **93**, 6987.

41. **(a)** G. Liu, E. Miliordos, S. M. Ciborowski, M. Tschurl, U. Bosel, U. Heiz, X. Zhang, S. S Xantheas and K. H Bowen, *J. Chem. Phys.*, 2018, **149**, 221101. **(b)** G. Liu, S. M. Ciborowski, Z. Zhu, Y. Chen, X. Zhang and K. H. Bowen, *Phys. Chem. Chem. Phys.*, 2019, **21**, 10955-10960. **(c)** G. Liu, Z. Zhu, S. M. Ciborowski, I. R. Ariyarathna, E. Miliordos and K. H. Bowen, *Angew. Chem. Int. Ed.*, 2019, **121**, 7855-7859. **(d)** G. Liu, I. R. Ariyarathna, S. M. Ciborowski, Z. Zhu, E. Miliordos and K. H. Bowen, *J. Am. Chem. Soc.*, 2020, **142**, 51, 21556-21561.

42. M. J. Frisch, G. W. Trucks and H. B. Schlegel, et al., GAUSSIAN09, Revision B.01, Gaussian, Inc., Wallingford, CT, 2004.

43. C. Adamo, V. Baron, *J. Chem. Phys.* 1998, **108**, 664 – 675, J. P. Perdew, *Electronic Structure of Solids*, Akademic Verlag: Berlin, Germany, 1991.

44. S. Paranthaman, K. Hong, J. Kim, D. E. Kim, and T. K. Kim, *J. Phys. Chem. A* 2013, **117**, 9293 – 9303.

45. D. J. Tozer and N. C. Handy, *J. Chem. Phys.* 1998, **109**, 10180.

46. X. Li, H. Wu, X. – B. Wang, and L. – S. Wang, *Phys. Rev. Lett.* 1998, **81**, 1909 – 1912

47. C. Y. Cha, G. Gantefor, and W. Eberhardt, *J. Chem. Phys.* 1994, **100**, 995 – 1010.

**Table 1.** Experimentally measured ADE, VDE values and calculated ADE and VDE values. All numbers are in eV.

| Systems | Expt. ADE | Theo. ADE | Expt. VDE | Theo. VDE |
|---|---|---|---|---|
| $LAl_5^-$ | ---- | 2.00 (isomer **3a**)<br>1.71 (isomer **3c**) | --- | 2.18 (isomer **3a**)<br>2.10 (isomer **3c**) |
| $LAl_6^-$ | 2.20 | 2.23 (isomer **5a**)<br>2.20 (isomer **5b**) | 2.60 | 2.52 (isomer **5a**)<br>2.40 (isomer **5b**) |
| $LAl_7^-$ | 1.90 | 1.96 (isomer **6a**)<br>1.90 (isomer **6b**) | 2.34 | 2.64 (isomer **6a**)<br>2.22 (isomer **6b**) |

## Figure Captions

**Figure 1.** Mass spectra of (a) bare aluminum cluster anions, $Al_n^-$, and (b) deprotonated HMDS-ligated aluminum cluster anions, $LAl_n^-$ (L = $N[Si(Me)_3]_2$).

**Figure 2.** Anion photoelectron spectra of $LAl_4^-$, $LAl_6^-$, and $LAl_7^-$ (L = $N[Si(Me)_3]_2$), taken with the third harmonic (355 nm wavelength) of a Nd:YAG laser.

**Figure 3:** The three lowest energy isomers of $LAl_5^-$ cluster, where L = $Ni[Si(CH_3)_3]_2$. The relative energies are given in eV.

**Figure 4:** The three lowest energy isomers of neutral $LAl_5$ cluster, where L = $Ni[Si(CH_3)_3]_2$. The relative energies are given in eV.

**Figure 5:** The lowest energy isomers of negatively charged and neutral $LAl_6$ clusters, where L = $Ni[Si(CH_3)_3]_2$. The relative energies are given in eV.

**Figure 6:** The lowest energy isomers of negatively charged and neutral $LAl_7$ clusters, where L = $Ni[Si(CH_3)_3]_2$. The relative energies are given in eV.

**Figure 7:** The four frontier molecular orbitals of $LAl_n^-$ (n = 5 – 7), where L = $Ni[Si(CH_3)_3]_2$.

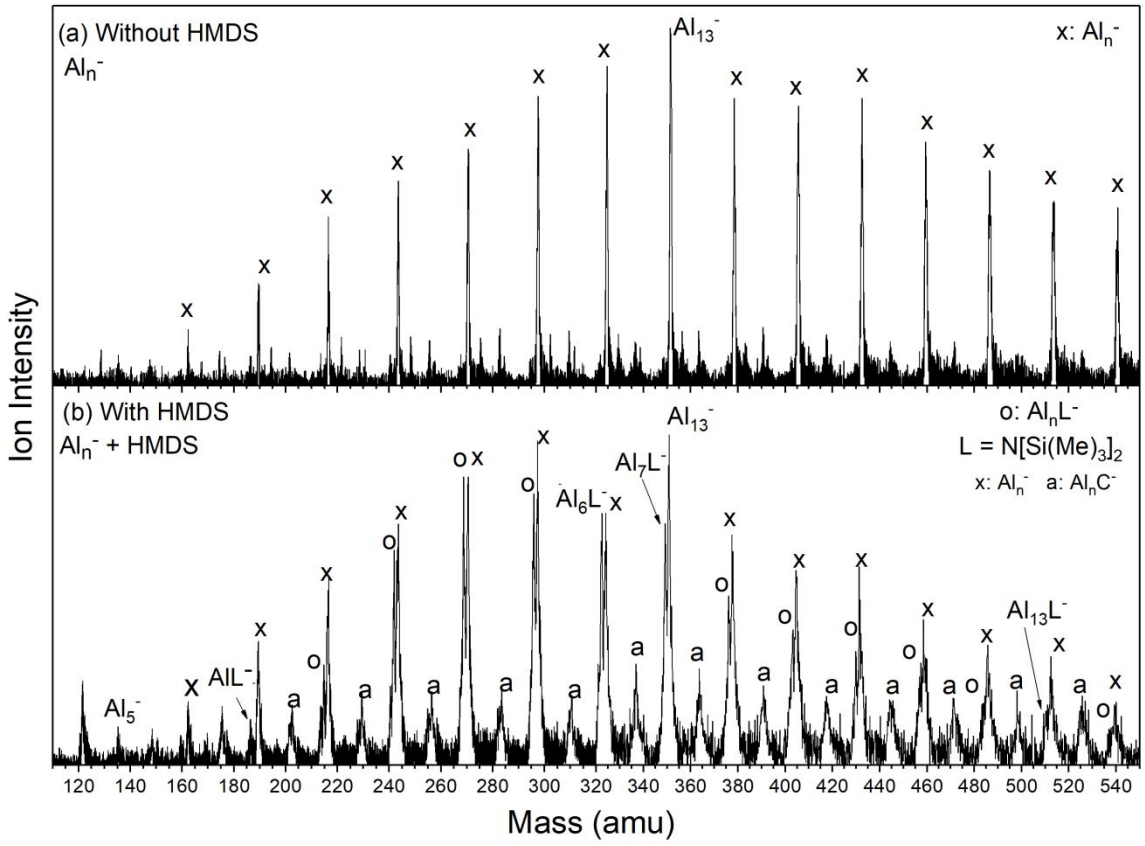
(a) Without HMDS
$Al_n^-$
x: $Al_n^-$
$Al_{13}^-$
(b) With HMDS
$Al_n^-$ + HMDS
o: $Al_nL^-$
L = $N[Si(Me)_3]_2$
x: $Al_n^-$ a: $Al_nC^-$
$Al_7L^-$
$Al_6L^-$
$AlL^-$
$Al_5^-$
$Al_{13}L^-$
Ion Intensity
Mass (amu)
120 140 160 180 200 220 240 260 280 300 320 340 360 380 400 420 440 460 480 500 520 540

**Figure 1**

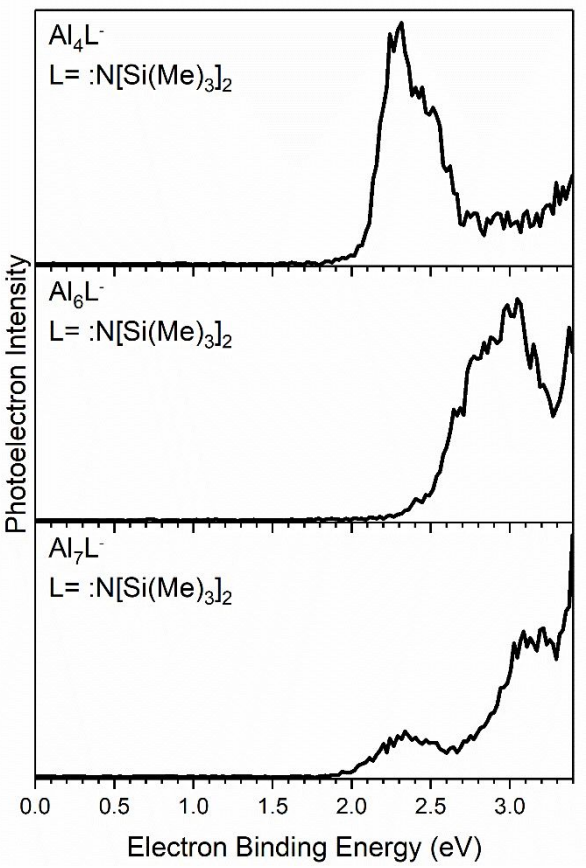
$Al_4L^-$
L= :N[Si(Me)$_3$]$_2$
$Al_6L^-$
L= :N[Si(Me)$_3$]$_2$
$Al_7L^-$
L= :N[Si(Me)$_3$]$_2$
Photoelectron Intensity
0.0
0.5
1.0
1.5
2.0
2.5
3.0
Electron Binding Energy (eV)

**Figure 2**

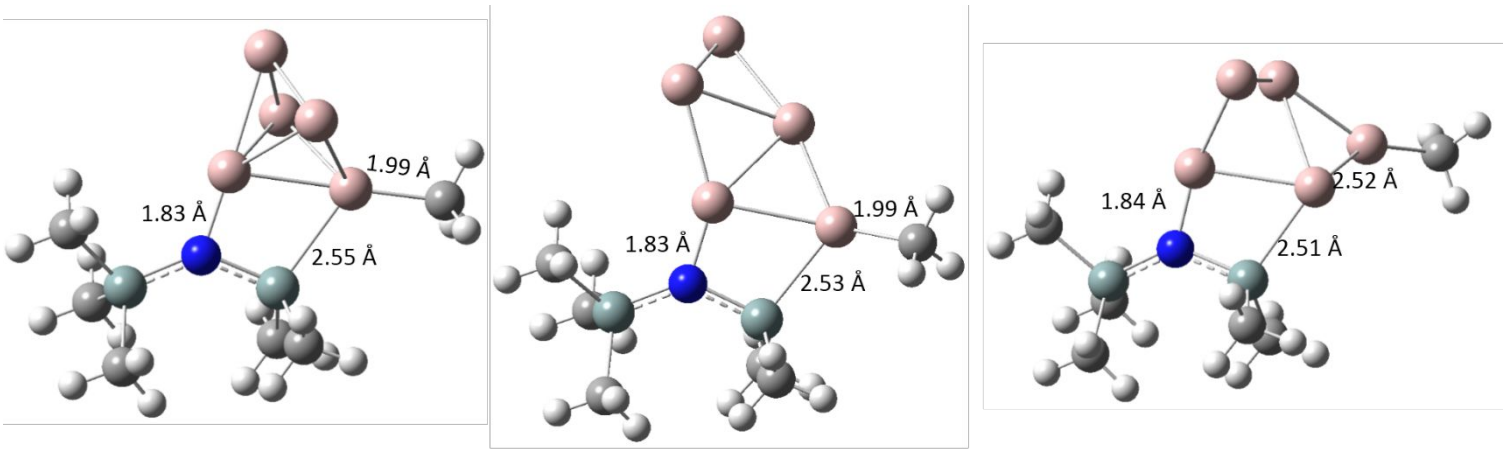


**(a)** ΔE = 0.00 eV **(b)** ΔE = 0.15 eV **(c)** ΔE = 0.16 eV

**Figure 3**

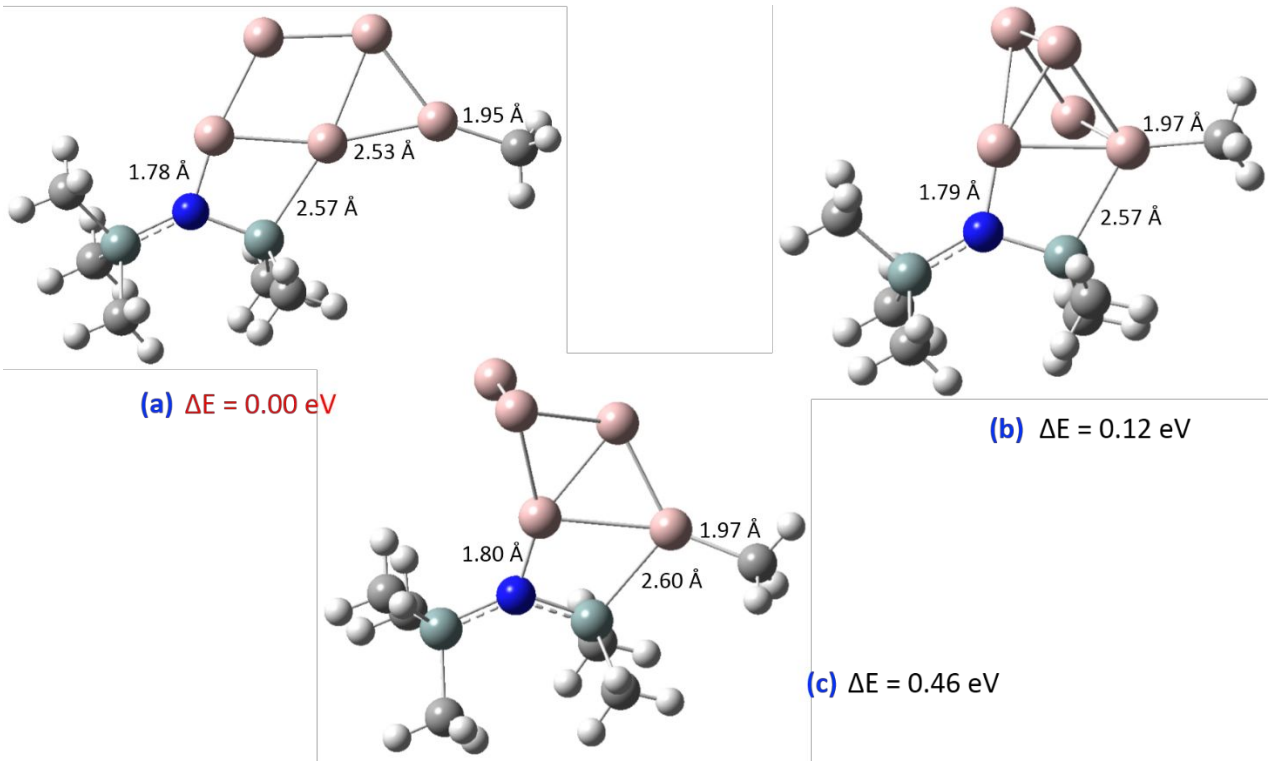
1.95 Å
2.53 Å
1.78 Å
2.57 Å
(a) ΔE = 0.00 eV
1.97 Å
1.79 Å
2.57 Å
(b) ΔE = 0.12 eV
1.97 Å
1.80 Å
2.60 Å
(c) ΔE = 0.46 eV

**Figure 4**

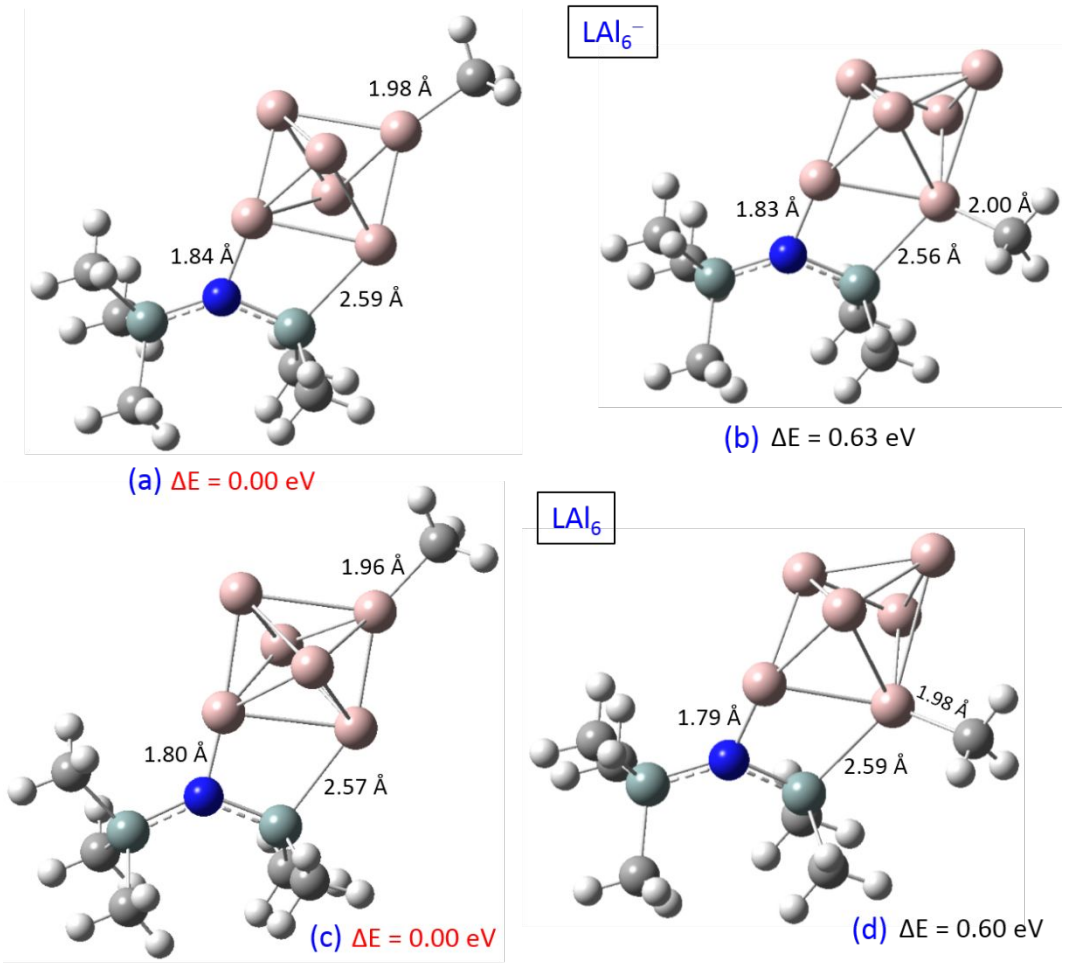
1.98 Å
1.84 Å
2.59 Å
(a) ΔE = 0.00 eV
LAl6−
1.83 Å
2.00 Å
2.56 Å
(b) ΔE = 0.63 eV
1.96 Å
1.80 Å
2.57 Å
(c) ΔE = 0.00 eV
LAl6
1.79 Å
1.98 Å
2.59 Å
(d) ΔE = 0.60 eV

**Figure 5**

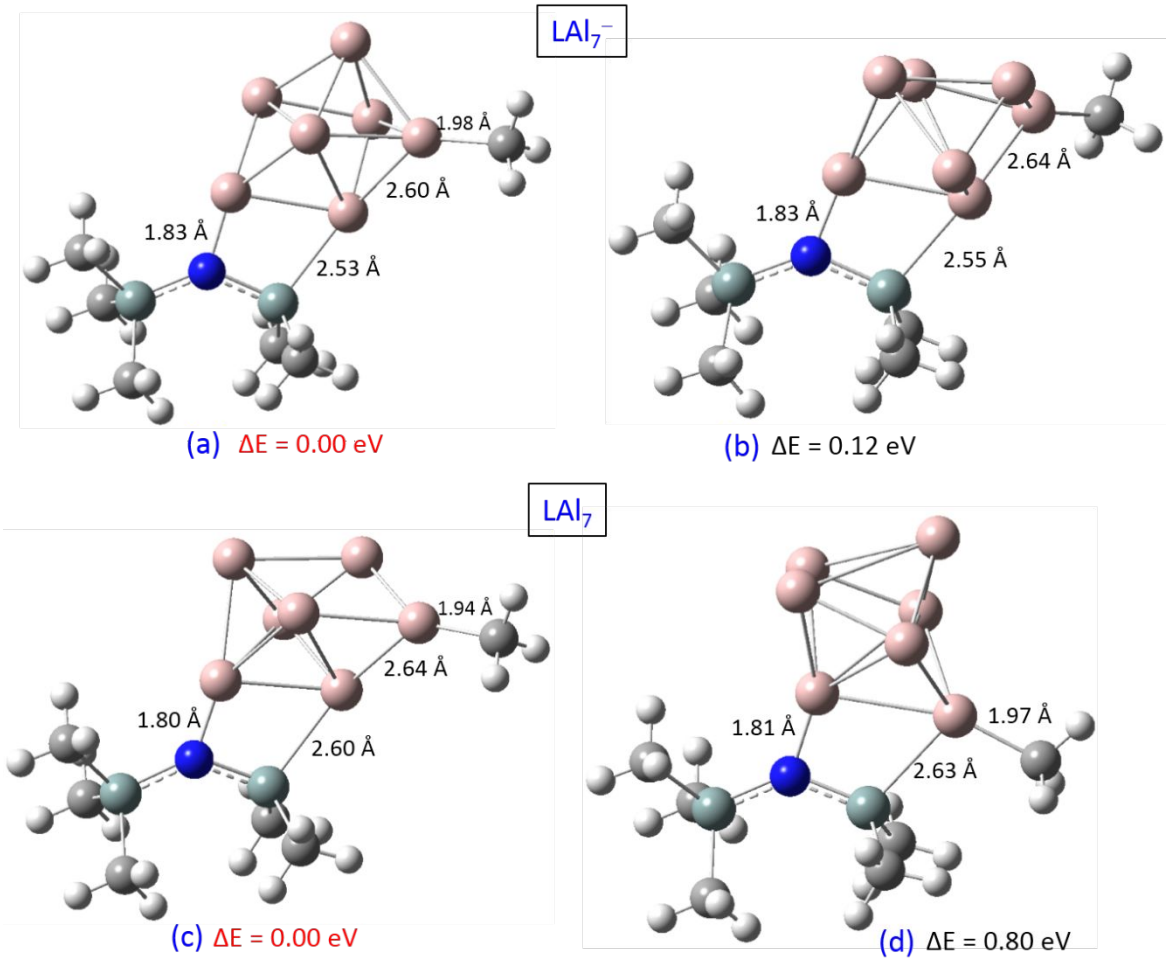
LAl7−
1.98 Å
2.60 Å
1.83 Å
2.53 Å
(a) ΔE = 0.00 eV
2.64 Å
1.83 Å
2.55 Å
(b) ΔE = 0.12 eV
LAl7
1.94 Å
2.64 Å
1.80 Å
2.60 Å
(c) ΔE = 0.00 eV
1.81 Å
1.97 Å
2.63 Å
(d) ΔE = 0.80 eV

**Figure 6**

| | HOMO | HOMO – 1 | HOMO – 2 | HOMO – 3 |
|---|---|---|---|---|
| $LAl_5^-$ | 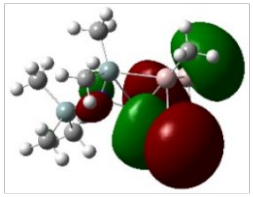 | 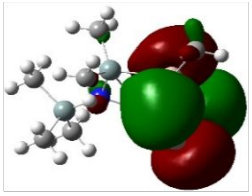 | 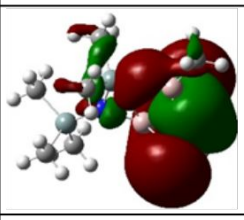 | 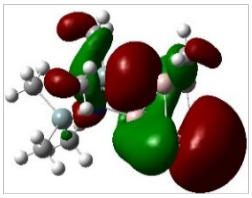 |
| $LAl_6^-$ | 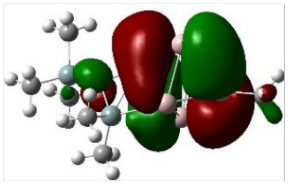 | 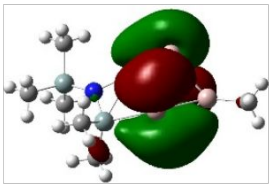 | 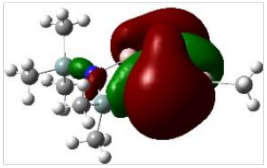 | 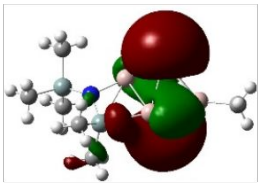 |
| $LAl_7^-$ | 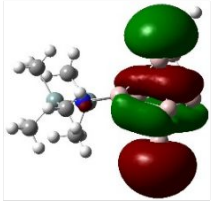 | 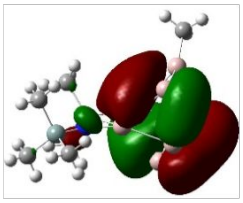 | 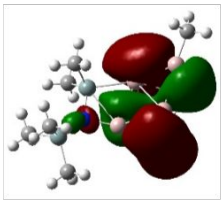 | 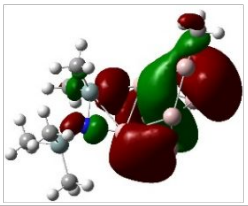 |

**Figure 7**